analytical chemistry

Article

Cite This: Anal. Chem. 2019, 91, 4747−4754

pubs.acs.org/ac

Belt-Mounted Micro-Gas-Chromatograph Prototype for Determining Personal Exposures to Volatile-Organic-Compound Mixture Components

Junqi Wang,[†,∥] Nicolas Nuñovero,[‡,∥] Robert Nidetz,[§,∥] Seth J. Peterson,[⊥] Bryan M. Brookover,[⊥] William H. Steinecker,[⊥] and Edward T. Zellers*[,†,‡,∥]

[†]Department of Chemistry, University of Michigan, Ann Arbor, Michigan 48109, United States

[‡]Department of Environmental Health Sciences, University of Michigan, Ann Arbor, Michigan 48109, United States

[§]Department of Mechanical Engineering, University of Michigan, Ann Arbor, Michigan 48109, United States

[∥]Center for Wireless Integrated MicroSensing and Systems, University of Michigan, Ann Arbor, Michigan 48109, United States

[⊥]Targeted Compound Monitoring, LLC, Beavercreek, Ohio 45440, United States

Supporting Information

ABSTRACT: We describe a belt-mountable prototype instrument containing a gas chromatographic microsystem (μGC) and demonstrate its capability for near-real-time recognition and quantification of volatile organic compounds (VOCs) in moderately complex mixtures at concentrations encountered in industrial workplace environments. The μGC comprises three discrete, Si/Pyrex microfabricated chips: a dual-adsorbent micropreconcentrator−focuser for VOC capture and injection; a wall-coated microcolumn with thin-metal heaters and temperature sensors for temperature-programmed separations; and an array of four microchemiresistors with thiolate-monolayer-protected-Au-nanoparticle interface films for detection and recognition−discrimination. The battery-powered μGC prototype (20 × 15 × 9 cm, ∼2.1 kg sans battery) has on-board microcontrollers and can autonomously analyze the components of a given VOC mixture several times per hour. Calibration curves bracketing the Threshold Limit Value (TLV) of each VOC yielded detection limits of 16−600 parts-per-billion for air samples of 5−10 mL, well below respective TLVs. A 2:1 injection split improved the resolution of early eluting compounds by up to 63%. Responses and response patterns were stable for 5 days. Use of retention-time windows facilitated the chemometric recognition and discrimination of the components of a 21-VOC mixture sampled and analyzed in 3.5 min. Results from a "mock" field test, in which personal exposures to time-varying concentrations of a mixture of five VOCs were measured autonomously, agreed closely with those from a reference GC. Thus, reliable, near-real-time determinations of worker exposures to multiple VOCs with this wearable μGC prototype appear feasible.

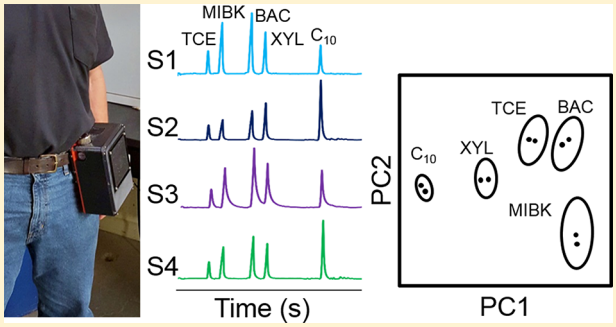

Volatile organic compounds (VOCs) are ubiquitous, and most are toxic to humans at sufficiently high concentrations. Health effects can range from mild narcosis and respiratory-tract irritation to dysfunction and disease in various organs and systems, including cancer.[1,2] The effects of exposure to mixtures of VOCs are not well-understood.[2,3] Exposure to VOCs is often higher in industrial workplaces because of the volumes of chemicals used, the nature of the activities performed, and the proximity of the workers to the sources of emission.[4] The collection of so-called *personal* measurements of worker exposures to toxic chemicals, ideally from the breathing zone, is mandated by regulations issued by the Occupational Safety and Health Administration (OSHA)[5] and guidelines issued by the National Institute for Occupational Safety and Health (NIOSH)[6] and the American Conference of Governmental Industrial Hygienists (ACGIH).[7]

For VOC mixtures, this typically entails collecting air samples with passive or active adsorbent-containing sampling devices clipped to the lapel of a worker for several hours, followed by subsequent laboratory analysis.[8] Obtaining measurements over shorter time intervals (i.e., minutes) could help identify high excursions, which may have health implications.[2,9] This is difficult because quantitative measurements of the individual components of VOC mixtures in near-real-time are only possible with field-portable or -transportable instruments employing gas chromatography with single-channel or mass-spectrometric detectors (GC or GC-MS)[10−12] or Fourier-transform infrared spectrophotometry

Received: January 15, 2019
Accepted: March 6, 2019
Published: March 6, 2019

DOI: 10.1021/acs.analchem.9b00263
Anal. Chem. 2019, 91, 4747−4754

(FTIR),[13] which are generally too large and expensive for routine or personal VOC-exposure monitoring. Smaller, highly sensitive GC-based instruments have become available more recently but appear to be limited by the nature and number of the compounds that can be determined in a single analysis.[14,15]

GC instruments made with Si-microfabricated components (μGC) offer the enticing possibility of measuring worker exposures to multiple specific VOCs in near-real time. Essentially, a μGC system suitable for analyzing airborne VOCs requires three (micro)analytical components: a collector−concentrator, which also functions as an injector, for sample capture and introduction; a chromatographic column for separation; and a sensor or sensor array for detection. Selected publications concerned with these components of possible μGC systems are listed in the Supporting Information (SI). Of course, additional means for transferring samples through the system and controlling system operations are also required to create a working instrument. Surprisingly few reports have appeared on functional systems or prototypes containing all three essential μGC components,[16−25] and a wearable μGC suitable for routine measurement of personal multi-VOC exposures has not yet been realized.

Building on prior work from our group,[19,23−28] we recently mounted an effort to develop μGC-based technology for which we coined the general term personal-exposure-monitoring microsystem (PEMM). The first-generation PEMM (PEMM-1) was a compact benchtop prototype,[25] built as a test bed for exploring design and operating features ultimately intended for incorporation into a second-generation prototype (PEMM-2). PEMM-1 employs a hybrid-integrated μGC analytical subsystem consisting of a dual-adsorbent micropreconcentrator−focuser (μPCF), tandem separation microcolumns (μSC), and an array of microchemiresistor (μCR) sensors coated with differently functionalized monolayer-protected-nanoparticle (MPN) films for recognition and quantification of eluting VOCs. The PEMM-1 prototype provided reliable, autonomous operation for ≥8 h, with low- or sub-parts-per-million (ppm) limits of detection (LOD) for targeted VOCs. However, it was AC-powered and tethered to a laptop computer for system control and data acquisition (i.e., not configured for personal-exposure monitoring).

Here, we report on the second-generation PEMM prototype (PEMM-2), which is one-third the size of its predecessor, PEMM-1; battery-powered; and equipped with on-board microcontrol hardware and software. This belt-mountable, fully packaged prototype is designed to simultaneously measure ∼10−20 VOCs 6−10 times per hour and store the data for subsequent assessment. The μPCF and μCR-array devices in PEMM-2 are of the same design as those developed for PEMM-1, but a more power-efficient, monolithic μSC replaces the PEMM-1 dual-μSC module.[25,28] Additional innovative features of the PEMM-2 (some also developed and validated via the PEMM-1) include a pretrap comprising a short wall-coated capillary for excluding intractable low-volatility interferences, a split-flow injector for increasing chromatographic resolution of early eluting VOCs, a streamlined fluidic layout, improved circuitry for sensor signal amplification and conditioning, on-board microcontrol of system functions and data acquisition, and a companion Raspberry Pi module for wireless communication. These and other improvements (discussed below) have resulted in lower LODs, more complex mixture analyses, enhanced vapor recognition, and lower operating power in the PEMM-2. Preliminary results of our PEMM-2 development effort have been described in two conference-proceedings papers.[29,30]

EXPERIMENTAL SECTION

Materials. The VOCs used for characterizing performance were as follows: benzene (BEN), trichloroethylene (TCE), *n*-heptane (C_7), 4-methyl-2-pentanone (MIBK), toluene (TOL), 2-hexanone (MBK), butyl acetate (BAC), ethylbenzene (ETB), *m*-xylene (XYL), 3-heptanone (EBK), *n*-nonane (C_9), α-pinene (PIN), cumene (CUM), *n*-propylbenzene (NPB), 1,2,4-trimethylbenzene (TMB), *n*-decane (C_{10}), *d*-limonene (LIM), nitrobenzene (NBZ), *n*-undecane (C_{11}), trichlorobenzene (TCB), and *n*-dodecane (C_{12}). These were purchased from Sigma-Aldrich/Fluka (Milwaulkee, WI) or Acros/Fisher (Pittsburgh, PA) in >95% purity (most >99% pure) and used as received. The graphitized-carbon adsorbents Carbopack B (C-B, 100 m^2/g) and Carbopack X (C-X, 240 m^2/g; Supelco, Bellefonte, PA) were manually sieved (212−250 μm) prior to loading into the μPCF. PDMS (OV-1) was obtained from Ohio Valley Specialty Company (Marietta, OH). MPNs (∼4 nm Au-core diameters) derived from the following thiols were used as μCR interface films: isooctyl-3-mercaptopropionate (EOE), *n*-octanethiol (C8), methyl-6-mercaptohexanoate (HME), 6-phenoxyhexane-1-thiol (OPH), and 1-mercapto-(triethylene glycol) methyl ether (TEG). TEG was purchased from Nanoprobes (3−5 nm core, Yaphank, NY). Other MPNs were from existing stocks synthesized by reported methods.[31,32] He gas canisters (>99.5%; 2500 PSI, 95 mL, 4.0 cm o.d. × 13 cm) and associated pressure regulator (Model 50047, NR24) were obtained from Leland (South Plainfield, NJ).

Microsystem Layout and Components. Figure 1a shows a block diagram of the core microsystem of the PEMM-2 prototype. Figure 1b−d show photographs of the three microfabricated analytical components: μPCF, μSC, and the μCR array, respectively. Figure 1e shows the assembled PEMM-2 with the cover removed to reveal the layout of the key components, the fluidic manifold, and the He canister. Detailed descriptions of the fabrication, mounting, packing and coating, and fluidic interconnections of the μPCF, μSC, and μCR-array devices have been published previously (consult refs 25 and 28), and therefore only salient features are recapitulated here.

The cavities and fluidic channels of the μPCF and μSC were formed in separate Si substrates by deep reactive ion etching (DRIE) and sealed with an anodically bonded Pyrex cap. For the μCR array, the substrate was Pyrex, and the cap was Si with a central channel formed by DRIE. Fluidic ports of all devices accepted 250 μm i.d. fused silica capillaries affixed with a flexible, high-temperature silicone adhesive (Duraseal 1531, Cotronics, Brooklyn, NY) or a rigid epoxy (Hysol 1C, Henkel Corporation, Rocky Hill, CT). Thin-film Ti/Pt resistive heaters and resistance temperature detectors (RTD) were patterned on the backsides of the devices.

The μPCF chip (Figure 1b, 1.4 × 4.1 cm footprint) has two ∼4.7 μL cavities flanked by rows of pillars to retain the adsorbent materials (2.0 mg C-B, 2.3 mg C-X, determined gravimetrically), which were loaded by gentle suction through side-ports subsequently sealed with Duraseal. The tee junction in the fluidic inlet channel allows vapor-sample loading through one branch (via mini-pump) and back-flushed injection (via He carrier gas) through the other. The device

DOI: 10.1021/acs.analchem.9b00263
Anal. Chem. 2019, 91, 4747−4754

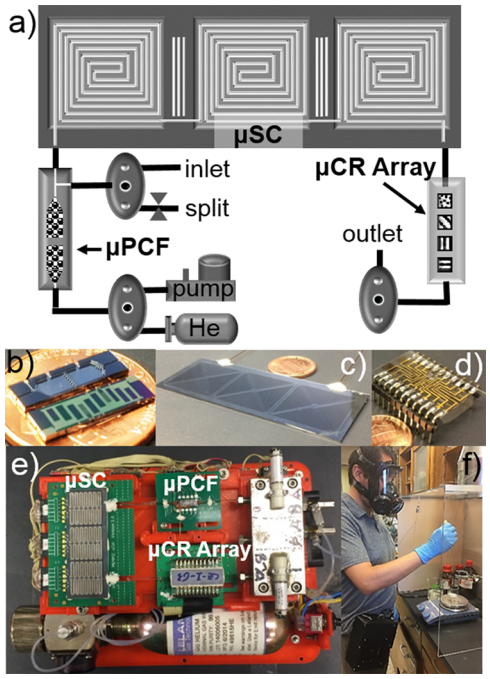

Figure 1. (a) PEMM-2 fluidic-layout diagram. (b) Micropreconcentrator–focuser (μPCF). (c) Microseparation column (μSC). (d) Microchemiresistor array (μCR array). (e) Fully assembled PEMM-2 with lid removed. (f) Belt-mounted PEMM-2 during setup for mock field tests.

was inverted, mounted, and wire-bonded to a custom printed circuit board (PCB).

The μSC chip (Figure 1c, 7.1 × 2.7 cm footprint) has a channel (6 m long, 250 × 140 μm cross section) divided into three 2 m long spiral segments. A 0.2 μm thick wall coating of PDMS was deposited statically and cross-linked thermally by a known method.[33] The chip has through-wafer (DRIE) slots between each segment and around its periphery for thermal isolation.[29] Three independent backside meander-line heaters were designed to minimize temperature gradients and power dissipation. The chip was inverted, mounted, and wire-bound to a PCB. Note that this μSC has a smaller footprint, fewer interconnections, and lower power consumption than the dual-μSC module used in the PEMM-1 prototype. Results of efficiency testing are presented in the SI.

The μCR-array chip (Figure 1d, 3.3 × 2.0 × 0.05 cm) has 10 sets of adjacent Au–Cr (300/30 nm) interdigital electrodes (IDEs), with a central Au–Cr RTD. Each μCR contains 27 electrode pairs, 5 μm wide with 4 μm gaps, and a 210 μm overlap. The Si lid has a 150 × 350 μm (diameter × width) channel down the center (above the linear array of IDEs). MPNs were drop-cast from solution to create (nonuniform) multilayer films with baseline resistances of 0.1 to 10 MΩ. Films of selected MPNs were cast on the IDEs, but only four μCRs were used per analysis because of imposed limitations on data acquisition channels in the prototype. The lid was sealed to the substrate with 0.05 cm thick strips of double-sided tape (VHB, 3M, St. Paul, MN) and an outer bead of Hysol. Right-angle metal pins were soldered to the bonding pads and plugged into a socket mounted on a custom PCB.

Prototype Assembly. A 3D-printed plastic platform supports each microsystem component on its respective PCB, elevated to a common plane on stand-off bolts. The μPCF and μCR-array PCB stand-offs fit into slide mounts for facilitating fluidic connections. The machined stainless-steel flow manifold (Figure 1e) has ports machined to accept the three gasket-sealed, three-way, latching solenoid valves (Model LHLA1221111H, Lee Company, Westbrook, CT). The capillaries emanating from the μPCF and μCR array connect to the appropriate manifold ports with zero-dead-volume fittings (Valco, Houston, TX) and to the μSC with press-tight connectors (Supelco). The pretrap consists of a 6.5 cm segment of a PDMS-coated capillary column,[25] and is mounted to the inlet port of the prototype with a threaded fitting. A set of four minifans installed above the microsystem components (not shown) provides cooling between cycles. A diaphragm mini-pump (NMP-09M, KNF, Reiden, Switzerland) is bolted beneath the manifold. Miniature needle valves (Beswick, Greenland, NH) mounted upstream of the mini-pump and downstream of the μPCF permit manual adjustment of the sampling flow rate and injection-split-flow ratio, respectively. The He canister is secured to the floor of the enclosure, and a separate rechargeable battery pack wired to the unit provides primary operating power (the μCR sensors were powered by a 3 V Li-ion coin cell). Four PCBs stacked under the microsystem platform contain the microcontrollers and other electronic components for running the prototype autonomously from a customized set of downloaded parameters. Please refer to the SI for a description.

System Control and Data Acquisition. A Raspberry Pi (RP) minicomputer module (12 × 8 × 2.5 cm, Raspberry Pi Foundation, Cambridge, U.K.) with wireless capability was mounted to the side of the PEMM-2 with Velcro. The RP stored the acquired data, and served as an interface between the embedded microcontrollers and a remote laptop computer connected to the same local network. A custom web graphical user interface allowed communication with the laptop for adjusting controls and monitoring the μCR-array output during testing. The PEMM-2 hardware supports autonomous operation; however, data retrieval, set-point and timing adjustments, and real-time updates require the RP.

Prior to any set of experiments, the operating parameters of the instrument, including the RTD-calibration factors, μPCF and μSC temperature programs, μCR reference-resistance matching, and timing of the modes of operation within a run, were entered in an Excel macro, converted to a machine-readable configuration file, and uploaded to the PEMM-2 system memory via a USB link. Additional details are in the SI.

Sample Preparation and Calibration. Test atmospheres of the VOCs were generated in 10 L Flex-foil gas sample bags (Supelco) by injecting the appropriate volume of each liquid and diluting with 8 L of N_2. Concentrations were approximately 0.1, 0.5, and 2 times the respective ACGIH 8 h Threshold Limit Value (TLV-TWA) for each vapor (see Table 1). By collecting (triplicate) samples of 5 and 10 mL (at 5 mL/min) with the PEMM-2, a 40-fold concentration range was spanned for each VOC. For verification, parallel samples drawn through a 250 μL sample loop (via a six-port valve) were injected into the inlet of a bench-scale GC-FID (7890B, Agilent Technologies, Santa Clara, CA) equipped with a short commercial (PDMS-coated) capillary column for separation and analysis. The concentrations (injected masses) were confirmed by reference to calibration standards prepared from mixtures in CS_2 and analyzed by GC-FID. For stability tests, replicate analyses were conducted over different time periods.

DOI: 10.1021/acs.analchem.9b00263
Anal. Chem. 2019, 91, 4747–4754

Table 1. Set of Nine VOCs and Their p_v Values, TLV Values, and Measured LODs

				LOD[a] (ppb)			
peak[b]	compd	p_v[c] (kPa)	TLV[d] (ppm)	C8	EOE	HME	TEG
1	BEN	12.6	0.5/2.5	150	140	600	550
2	C_7	6.13	400/500	180	110	170	300
3	TOL	3.78	20/–	110	100	460	430
4	MBK	1.55	5/10	89	60	58	170
5	BAC	1.53	50/150	65	49	90	230
6	XYL	1.01	100/150	92	78	330	330
7	EBK	0.533	50/75	100	50	58	220
8	NPB	0.456	–[e]	51	68	88	100
9	TMB	0.270	25/–	33	43	63	66

[a]Lowest detectable air concentration derived from mass-based LOD assuming a 5 mL air-sample volume. Acronyms are defined in the Experimental Section. [b]Peak assignments for the chromatograms in Figure 2. [c]At 25 °C. [d]The 8 h TLV-TWA is listed first, and the 15 min TLV-STEL is listed second (if assigned).[7] [e]No assigned TLV.

Mock-Field-Test Setup. Mock field tests were conducted by use of a custom benchtop enclosure made of Plexiglas (61 × 60 × 43 cm, width × height × depth) with an open front panel and a variable-speed, ceiling-mounted exhaust fan that vented to a lab hood. For the tests reported below, liquid TCE, MIBK, BAC, XYL, and C_{10} were mixed in a 250 mL beaker. Small aliquots of the mixture were transferred by pipet to a second beaker on a hot plate–stirrer at different times and temperatures to induce vapor-concentration fluctuations. The research-team member wore a properly fit-tested air-purifying respirator, and the VOC concentrations measured at the face of the chamber were maintained below their respective 8 h TLV-TWA and 15 min TLV short-term-exposure-limit (TLV-STEL) levels.[7]

The PEMM-2 (with RP) was clipped to the belt of the researcher on the right hip, and the battery pack was placed in the left front pocket. A deactivated capillary extension to the pretrap allowed collection of samples near the breathing zone. For reference, parallel samples were drawn through a colocated capillary connected to a six-port valve with a 250 μL sample loop mounted on a nearby bench-scale GC-FID.

Data Management and Processing. Raw chromatogram traces (i.e., μCR signals) could be stored in the PEMM-2 but, for testing, were instead transferred to the RP and then wirelessly to a laptop computer for display, storage, conversion of voltage readings to normalized resistance readings, and subsequent processing (see SI). Chromatograms were analyzed using OriginPro (Ver. 9.1, OriginLab, Northampton, MA). Regression models, calibration curves, response patterns, and other data plots were generated in Microsoft Excel. Principal-component analyses (PCA) were conducted in R (Ver. 3.4.0, R Foundation, Vienna, Austria). Monte Carlo (MC) simulations were implemented in Visual Basic. See the SI for MC-PCA procedures.

RESULTS AND DISCUSSION

Basic Operation. The assembled PEMM-2 measures 20 × 15 × 9 cm, and weighs 2.1 kg (sans battery pack). Thus, it is 66% smaller and 40% lighter than the PEMM-1.[25] The selections of μPCF adsorbent materials, μSC stationary phase, and MPNs in the μCR were based on prior development work.[25,27,34] A standard operating cycle entails the following steps: sample collection, injection, separation, multisensor detection–recognition, and reinitialization. First, the pump draws a preprogrammed volume of air in through the pretrap and μPCF. The pump is then turned off, valves are switched, and He gas is passed through the microsystem at 2–3 mL/min. Rapid heating of the μPCF to 225 °C desorbs the VOCs captured on the C-X or C-B adsorbents, which are then carried into the μSC in a sharp bolus with the option for split or splitless injection. After a temperature-programmed separation, eluting VOCs are detected by the resistance changes of the μCR sensors as the VOCs reversibly partition into the different MPN coating films, giving rise to a response pattern. While the μPCF and μSC are cooling, the He flow is then directed back through the pretrap to flush any retained compounds.

As with PEMM-1,[25,27] the target VOCs for which quantitative analysis would be possible were restricted to those with vapor pressures, p_v, in the range $0.03 < p_v < 13$ kPa, because lower-volatility compounds would tend to adhere to all unheated surfaces in the flow path, and higher-volatility compounds would not be completely trapped by the adsorbents in the μPCF. Furthermore, compounds with higher p_v values would be difficult to separate on the short μSC, and they would also be detected with lower sensitivity on the sorption-dependent μCR sensors. This concession acknowledges the inherent limitations of our system architecture and materials, as well as considerations of prototype size and power requirements. However, it also minimizes the capture of water vapor by excluding a higher surface adsorbent (e.g., a carbon molecular sieve[35]).

The nine VOCs in Table 1 were selected for the initial test mixture because their p_v values fall well within the stipulated range, they collectively represent several different functional-group classes, they were easily separable, and most had assigned TLV values. It was assumed that 0.1 × TLV to 4 × TLV represented a reasonable concentration range for which accurate quantification would be required.[27] For subsequent tests focused on vapor recognition, a set of 21 common workplace VOCs was selected that extended the range of compound p_v values to the limits designated above.

Calibration and LODs. A simple temperature program was established to permit baseline separation of the peaks corresponding to the selected set of nine VOCs in <120 s. Representative chromatograms from each of the four MPN-coated sensors in the μCR array are shown in Figure 2. As shown, peaks were generally symmetric, but tailing occurred, particularly from the sensors coated with the more polar TEG and HME MPNs. Asymmetry factors were <1.2 in most cases and <2.8 in all cases. Retention times (t_R), full widths at half-maximum (fwhm), and resolutions (R_s) under these conditions are listed in Table S-1 (SI). The peak eluting before BEN (i.e., peak 1) is attributable to trace levels of water vapor in the N_2 used to create the test atmosphere.

For calibration, the average peak area, A ($\Delta R/R_b \times s$), and peak height, H ($\Delta R/R_b$), were separately plotted versus injected mass. Linear regression with a forced-zero y-intercept ($R^2 > 0.99$ in all cases) yielded sensitivity values from the slopes of the lines (see Figure S-2 and Table S-2). Response patterns for all nine VOCs are presented as bar charts in Figure S-3. Although patterns could be analyzed, we have elected to address the matter of vapor recognition using the more complex 21-VOC-mixture data presented below.

LODs, estimated from the regression models (H vs injected mass) and typical baseline noise values of each sensor, are compiled in Table S-2. These mass-based LODs ranged from

DOI: 10.1021/acs.analchem.9b00263
Anal. Chem. 2019, 91, 4747–4754

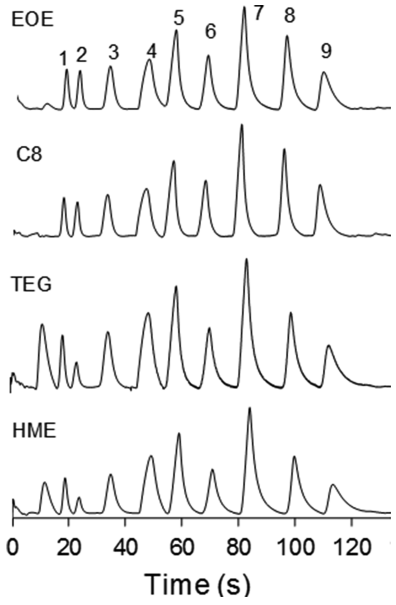

Figure 2. Nine-VOC chromatograms (voltage readings) from PEMM-2. Conditions: ~100 ppm of each vapor, 2.5 mL of sample at 5 mL/min, splitless injection at 2 mL/min He carrier gas, μPCF at 225 °C for 40 s, μSC temperature program of 30 °C for 35 s and then 40 °C/min to 105 °C, and μCR array at 30 °C. Peaks: 1, BEN; 2, C_7; 3, TOL; 4, MBK; 5, BAC; 6, XYL; 7, EBK; 8, NPB; 9, TMB.

1.2 ng (i.e., TMB with the C8 sensor) to 9.5 ng (i.e., BEN with the HME sensor). In terms of air concentrations (Table 1), LODs ranged from 33 ppb (TMB, C8 sensor) to 600 ppb (BEN, HME sensor) assuming a 5 mL air sample. The LODs for a given VOC differ by ≤5-fold among the sensors in the array, whereas the LODs for a given sensor differ by ≤10-fold among all VOCs.

All compounds could be detected by all sensors at ≪0.1 × TLV-TWA concentration levels, except BEN, for which the LODs with the HME and TEG sensors were somewhat higher than this threshold. This is due to the low TLV-TWA for benzene (i.e., 0.5 ppm) and to its high p_v value and low polarity, both of which limit partitioning into these polar MPN films. If the sample volume were increased to 10 mL, then the LODs would be <0.1 × TLV-TWA for all vapor−sensor pairs. Of course, all LODs are ≪0.1 × TLV-STEL with the default 5 mL sample volume. These LODs are lower than those obtained with the PEMM-1 prototype for VOCs common to both studies,[25] owing apparently to the sharper peaks obtained by use of the new, monolithic μSC and the more streamlined fluidic pathways in PEMM-2.

Stability of Responses and Response Patterns. Values of *A*, *H*, and t_R of the nine VOCs were compiled, and the relative standard deviations (RSD) around the different average values were used for assessment of short-term (i.e., 30 min), intraday (i.e., 8 h), and interday (i.e., 5 day) stability of responses for samples collected from the same test atmosphere. Detailed results are presented in Figure S-4 and Table S-3 for the (representative) EOE sensor.

In summary, the short-term stability was excellent for all three measured parameters over 30 min (n = 6 consecutive 5 min measurements): all RSD values were <2.5%, and most were <2.0%. Intraday stability (n = 6 time-separated measurements over 8 h each day for 5 days) was also very high, with RSD values ≤5.0% in all cases and <2.0% in most cases. The interday stability (n = 5 daily average measurements over 5 days) was lower for all three parameters, with RSD values as high as 7.7% for *A* and ~6% for *H* and t_R. Notably, the reference GC-FID responses (n = 5 individual measurements over 5 days, loop injections) gave interday RSDs for *A* and *H* comparable to those for the PEMM-2, suggesting that a portion of the variation may be attributable to small changes in ambient temperature or pressure causing changes in the absolute concentrations of the VOCs in the bag.

The interday stability of the response patterns was investigated by use of MC-PCA. The response vector (from peak areas) obtained from the sum of the responses of the four μCR sensors for each vapor on day 1 was used as the reference point, and the 95% confidence interval (CI_{95}) around that pattern was established for each VOC by use of MC simulations that assumed an average random error of 5% for each sensor in the array. Response vectors from measurements collected on subsequent days were then evaluated relative to this CI_{95}. Of the 36 data points (i.e., 4 days × 9 VOCs) only three fell (barely) outside of their respective CI_{95} ranges (see Figure S-4b).

21-VOC Mixture. For the analysis of the more complex 21-VOC mixture, a new μCR array was installed wherein OPH was substituted for TEG because of a persistent baseline-resistance drift in the previous TEG-sensor output. After optimizing the separation conditions, the influence of split-flow injection was evaluated, and then the utility of combining a retention-time window approach to parsing the chromatogram with chemometric analysis of array responses for vapor recognition was explored.

Figure 3 shows the set of 21-VOC chromatograms obtained from the four μCRs in the array along with the reference GC-FID separation performed under similar conditions. The p_v range spanned by the analytes is 430-fold: from ~13 kPa (BEN) down to 0.03 kPa (C_{12}). Retention times were assigned during preliminary tests with subsets of compounds. A 1 min sample was collected at 5 mL/min; the μPCF was heated and backflushed at 9 mL/min with a 2:1 injection-split ratio so that the flow through the μSC was 3 mL/min. The temperature-programmed separation required about 150 s.

Several features of the chromatograms (Figure 3b) are noteworthy. First, the peak shapes from three of the four sensors are quite symmetric, the exception being the OPH sensor, which shows significant tailing that degrades the quality of the separation. This MPN was found later to have exhibited partial agglomeration in the vial in which it was stored, which could account for the apparently slower responses to vapor sorption−desorption. This notwithstanding, the overall separation quality is quite good, with near-baseline separation achieved for most analytes. Exceptions include the full or partial binary coelutions of peaks 2/3, 4/5, 8/9, and 10/11. Although broader peaks are expected for later-eluting compounds, and the finite dead volume of the CR-array headspace may be a factor, it is clear from a comparison with the GC-FID trace (Figure 3a) that the VOC-MPN sorption−desorption rates contribute significantly to peak broadening and some loss in resolution for the late eluters (e.g., peaks 18−21).[26]

For fully or partially coeluting peak pairs, the array response patterns may help to resolve the identities of the compounds in the pair. To explore this, we chose the four binary coelutions cited above (Figure 3) and applied MC-PCA to the composite responses. Figure 4a−d shows PC score plots for these

DOI: 10.1021/acs.analchem.9b00263
Anal. Chem. 2019, 91, 4747−4754

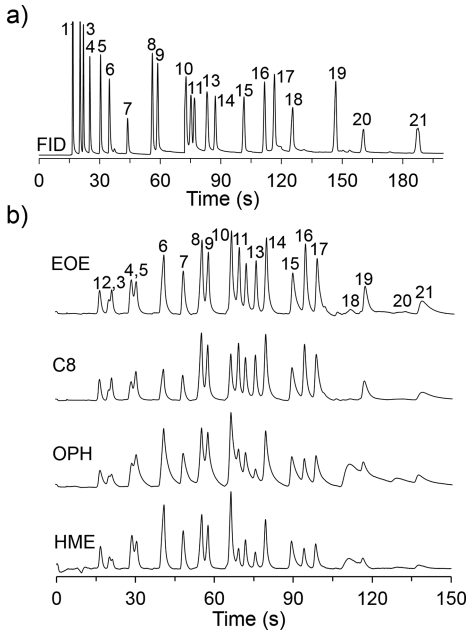

Figure 3. 21-VOC chromatograms. (a) GC-FID (250 μL loop injection; temperature program: 30 °C for 36 s, then 50 °C/min to 115 °C, hold). (b) Four μCR-array sensors in PEMM-2 (baseline corrected; sample at 5 mL/min for 1 min; 2:1 split injection with 3 mL/min He flow through μSC; μPCF, 225 °C for 40 s; μSC temperature program: 30 °C for 50 s, then 50 °C/min to 125 °C, hold). Peaks: 1, BEN; 2, TCE; 3, C_7; 4, MIBK; 5, TOL; 6, MBK; 7, BAC; 8, ETB; 9, XYL; 10, EBK; 11, C_9; 12, PIN; 13, CUM; 14, NPB; 15, TMB; 16, C_{10}; 17, LIM; 18, NBZ; 19, C_{11}; 20, TCB; 21, C_{12}. Test atmosphere: ~100 ppm of each VOC except NBZ (~50 ppm) and TCB (~10 ppm).

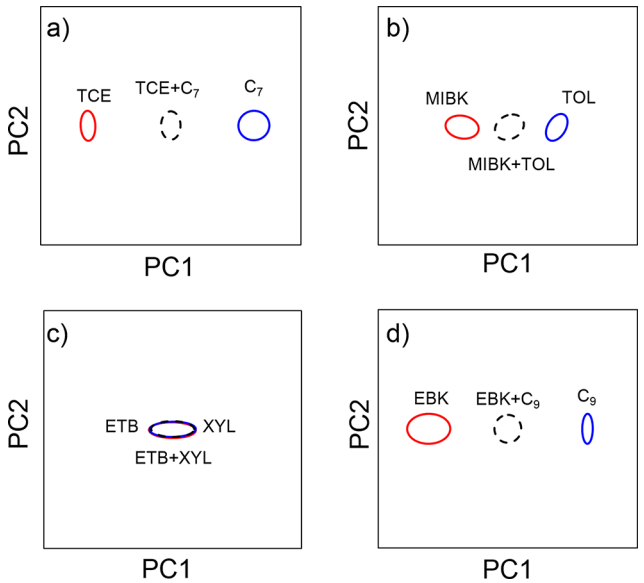

Figure 4. Principal-component score plots derived from μCR-array response patterns for the four pairs of compounds with fully or partially coeluting peaks in Figure 3. Ellipses correspond to the projected CI_{95} ranges around the calibrated patterns (vectors) for each vapor (solid lines) in 1:1 mixtures (dashed lines).

compound pairs for which R_s ranged from 0.4 to 1.3. The elliptical region plotted for each compound is the projected CI_{95} around its response vector derived from MC-PCA, again assuming 5% random variation in each sensor response. Also included is the projected CI_{95} of the 1:1 mixture of each pair (dashed lines).

As shown, for three of the four pairs, the vector for one member is well-separated from that of the other member and from the mixture (i.e., no overlap of CI_{95}), indicating that compounds in these pairs could be differentiated even if their peaks fully overlapped. The exceptional pair is ETB and XYL (Figure 4c), which cannot be resolved chemometrically because they are isomers, and their partitioning behaviors will be nearly identical for all sensors. Thus, only a composite measure of their exposure concentrations could be obtained.

The use of a modest 2:1 injection split resulted in significant improvements in chromatographic resolution, albeit at the expense of sensitivity (2/3 of the sample mass is vented).[27] Figure 5a,b compares the chromatograms for the 21-VOC

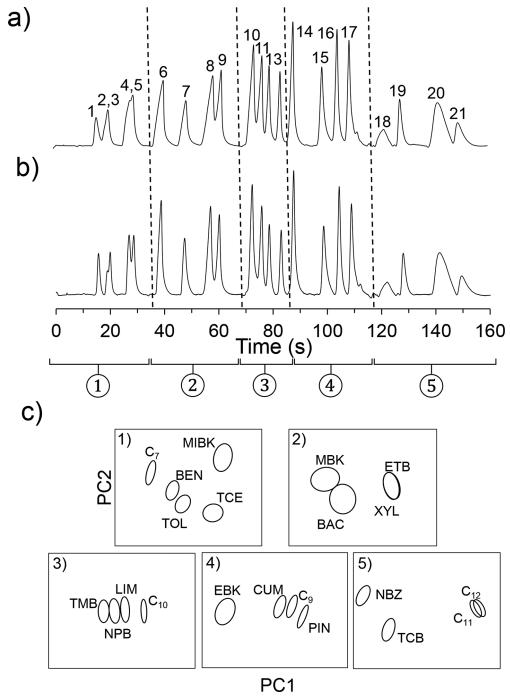

Figure 5. Twenty-one-VOC chromatograms from the EOE sensor in PEMM-2 with (a) splitless and (b) 2:1 split injection. The conditions are the same as in Figure 3, except the μSC maximum temperature was 110 °C. (c) PC score plots for compounds falling within retention-time windows defined by the dashed lines in (a), where the elliptical region for each VOC represents the CI_{95} around its pattern (vector).

mixture with and without the split, respectively, on the basis of the EOE sensor output. The split injection did not change the t_R value for any compound, but the fwhm values decreased by as much as 40%. The effect is much more prominent for the early eluting compounds. For example, the fwhm of BEN (peak 1) decreased by 40% (from 1.7 to 1.0 s) and that for MBK (peak 6) decreased by 20% (from 2.0 to 1.6 s) with the split. Additional peak narrowing is observed to a progressively lesser extent out to NPB (peak 14, 6%), beyond which there is little or no impact.

Accordingly, the resolution of adjacent peaks in the first part of the chromatogram is enhanced. Thus, the R_s for ETB (peak 8) and XYL (peak 9) increased by 63% (from 0.8 to 1.3) with the split, but the R_s for TMB (peak 15) and C_{10} (peak 16) remained at 2.1 despite the split. This is consistent with the

DOI: 10.1021/acs.analchem.9b00263
Anal. Chem. 2019, 91, 4747−4754

expectation that compounds with lower vapor pressures (i.e., below ~0.5 kPa) will exhibit on-column focusing with an initial column temperature of 30 °C, such that there is little or no benefit from a sharper injection. In contrast, more volatile compounds do not spontaneously focus, and their resolution is strongly dependent on the injection bandwidth.

Returning now to the entire set of four chromatograms from PEMM-2 for the 21-VOC mixture, we first performed an MC-PCA on the data set without regard for chromatographic separations. The PC score plot in Figure S-5 shows that the patterns for some compounds are well-separated (i.e., differentiable as individual VOCs), whereas many others are not. Recognizing all components of this mixture on the basis of array response patterns alone is not possible.

The approach we took to incorporating retention-time information into the analysis entailed dividing the chromatogram into retention-time windows containing subsets of compounds, and then performing vapor-recognition analyses on each subset sequentially.[16] For illustration, we arbitrarily chose to divide the chromatogram into five windows, each containing 4−5 compounds, as indicated by the dashed lines in Figure 5a,b. MC-PCA was then conducted within each window.

Results are shown graphically in Figure 5c. For the first window (Figure 5c-1, compounds 1−5), the pattern separation is excellent, indicating that the identities of the compounds could be confirmed as long as all peaks are resolved chromatographically. Certain binary coelutions could be tolerated, as shown above for the case of BEN and C_7, but additional testing would be needed to assess which other coeluting pair patterns could be separated. (In general, ternary coelutions cannot be resolved on the basis of their array response patterns.[36]) For the second window (Figure 5c-2), MBK and BAC are sufficiently separated from each other and from ETB and XYL for effective vapor recognition. Per above, however, ETB and XYL cannot be differentiated. For the third and fourth windows (Figure 5c-3,4), once again all VOC patterns are well-resolved. For the last window (Figure 5c-5), not surprisingly, the C_{10} and C_{11} patterns overlap. Fortunately, adjacent members of homologous series such as these are always well-resolved chromatographically. Thus, despite being in the same window, their peaks are well-separated (Figure 5a), and they are thereby differentiable. Note that constraining the pattern library to only those VOCs within a designated window greatly facilitates recognition via response patterns. Single-channel detectors lack the capability to confirm compound identities.

Mock Field Test. PEMM-2 conditions were adjusted so that the mixture of five VOCs could be sampled and analyzed every 5 min. Figure 6 shows representative 60 min exposure profiles for one of the VOCs (i.e., TCE) from the PEMM-2 and reference GC-FID for the individual wearing the PEMM-2 while he was engaged in solvent-transfer activities. The inset in Figure 6 shows a representative set of chromatograms. Profiles for all five VOCs are presented in Figure S-6.

The ranges of concentrations spanned from 9- to 40-fold among the five VOCs, but remained below TLV values. In general, the PEMM-2 and GC-FID concentrations agreed quite closely, and the spatial and temporal variability in the actual VOC concentrations could account for differences observed at a given point in time. The error bars bracketing the GC-FID measurements correspond to RSD values ranging from 6 to 76% (most from 10 to 30%), indicating occasionally

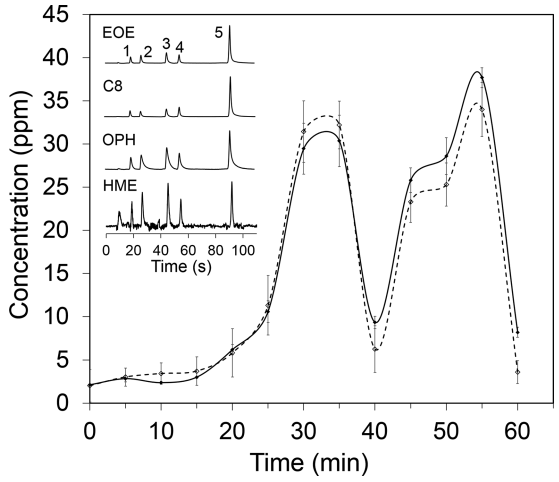

Figure 6. Representative time-exposure profiles for one of the five VOCs (i.e., TCE) over 60 min of continuous, unattended operation of PEMM-2 (solid line) while worn on the belt of one of the research-team members, along with the reference measurements by GC-FID (dashed line). Two GC-FID samples were analyzed during each 1 min sampling period of PEMM-2. Each data point is the average of either four sensors from PEMM-2 or two analyses from GC-FID. Error bars depict standard deviations. The inset shows representative PEMM-2 chromatograms (at t = 50 min). Peaks: 1, TCE; 2, MIBK; 3, BAC; 4, XYL; 5, C_{10}. Activities are described in the caption of Figure S-6.

large concentration fluctuations between sequential 30 s samples. Concentration estimates from the PEMM-2 sensors at a given point in time varied by ≤13% (RSD), and response patterns were also quite stable, with ~85% of the 60 vectors falling within the CI_{95} and no errors in assigned identities (see Figure S-6f).

Power and Energy. The average power consumption for a typical cycle (i.e., 1 min for sampling, 2.5 min for analysis, and 2.5 min for cooling and resetting) is only 5.8 W, which is 68% of that for the PEMM-1 prototype (see Table S-4). The energy per 6 min cycle is only 2.1 kJ and is dominated by the electronics. Thus, a battery with a capacity of <50 W h should permit operation for at least 8 h.

CONCLUSIONS

We conclude that the PEMM-2 prototype, employing a core analytical subsystem made entirely from Si-glass microfabricated components, is well-suited for measuring near-real-time worker (personal) exposures to the components of moderately complex multi-VOC mixtures at concentrations encountered in industrial environments. The capability for recognizing and quantifying VOC-mixture components embodied in the PEMM-2 is not available in current wearable monitoring instrumentation and has not been reported in the literature. MPN film quality and stability could be improved with greater care in synthesis, storage, and film deposition. Further reductions in size and weight could be achieved readily by incorporating a smaller (custom) He canister and regulator and a smaller and lighter valve manifold. Reductions in power should be possible by implementing sequential heating of the μSC segments.[28] On-going work is focused on demonstrating unattended (battery) operation for 8 h and testing in actual workplaces.

DOI: 10.1021/acs.analchem.9b00263
Anal. Chem. 2019, 91, 4747−4754

■ ASSOCIATED CONTENT

Supporting Information

The Supporting Information is available free of charge on the ACS Publications website at DOI: 10.1021/acs.analchem.9b00263.

Citations of literature on component devices of potential use in μGC systems, determination of μSC separation efficiency, components and features related to PEMM-2 control and operating options, calibration metrics and response patterns for the nine VOCs, MC-PCA procedure for assessing VOC recognition, response-stability data, PC score plot from MC-PCA of the 21-VOC mixture, mock-field-test data, and power- and energy-consumption breakout for a typical cycle (PDF)

■ AUTHOR INFORMATION

Corresponding Author

*E-mail: ezellers@umich.edu. Tel.: 1-734-936-0766.

ORCID

Junqi Wang: 0000-0002-0006-0332

Edward T. Zellers: 0000-0003-2047-6367

Notes

The authors declare no competing financial interest.

■ ACKNOWLEDGMENTS

The authors sincerely thank the following individuals for their contributions to this study: Jonathan Bryant-Genevier and William Collin (early design and assembly), Kee Scholten and Changhua Zhan (μCR-array design and fabrication), Chengyi Zhang and Jialiu Ma (MPN synthesis), Zhijin Lin (initial mock field testing), and Professor Katsuo Kurabayashi and Sanketh Buggaveeti (guidance in design and fabrication of μPCF and μSC). Devices were made in the Lurie Nanofabrication Facility. Funding was provided by NIOSH-CDC Grant R01-OH-010297. The authors are solely responsible for the content of this article.

■ REFERENCES

(1) Indoor Air Quality Scientific Findings Resource Bank: Volatile Organic Compounds. *Department of Energy National Laboratory*. https://iaqscience.lbl.gov/voc-summary (accessed Nov 2018).

(2) *Documentation of the TLVs and BEIs*, 7th ed.; American Conference of Governmental Industrial Hygienists: Cincinnati, OH, 2001, with annual supplements through 2018.

(3) Bruckner, J.; Anand, S.; Warren, D. A. Toxic Effects of Solvents and Vapors. In *Casarett and Doull's Toxicology: The Basic Science of Poisons*; Klaassen, C. D., Ed.; McGraw-Hill: New York, 2013; pp 1031−1132.

(4) Harper, M.; Weis, C.; Pleil, J. D.; Blount, B. C.; Miller, A.; Hoover, M. D.; Jahn, S. *J. Exposure Sci. Environ. Epidemiol.* **2015**, *25*, 381−387.

(5) Permissible Exposure Limits, OSHA Annotated Table Z-1. *Occupational Safety and Health Administration*. https://www.osha.gov/dsg/annotated-pels/tablez-1.html (accessed Nov 2018).

(6) *Pocket Guide to Chemical Hazards*; DHHS (NIOSH) Publication No. 2005-149; National Institute for Occupational Safety and Health, 2007. https://www.cdc.gov/niosh/docs/2005-149/pdfs/2005-149.pdf (accessed Nov 2018).

(7) *TLVs for Chemical Substances and Physical Agents & BEIs*; American Conference of Governmental Industrial Hygienists: Cincinnati, OH, 2018.

(8) Ashley, K., O'Connor, P. F., Eds.; *NIOSH Manual of Analytical Methods*, 5th ed.; National Institute for Occupational Safety and Health, 2017. https://www.cdc.gov/niosh/nmam/pdfs/NMAM_5thEd_EBook.pdf (accessed Nov 2018).

(9) Shen, D. D. Toxicokinetics. In *Casarett and Doull's Toxicology: The Basic Science of Poisons*; Klaassen, C. D., Ed.; McGraw-Hill: New York, 2013; pp 367−390.

(10) HAPSITE ER Chemical Identification System. *INFICON*. https://products.inficon.com/en-us/nav-products/product/detail/hapsite-er-identification-system/ (accessed June 2018).

(11) Micro GC Fusion Gas Analyzer. *INFICON*. https://products.inficon.com/en-us/nav-products/product/detail/micro-gc-fusion-gas-analyzer/ (accessed June 2018).

(12) zNose Portfolio. *Electronic Sensor Technology*. http://www.estcal.com/products (accessed Aug 2018).

(13) Portable DX4040 FTIR Gas Analyzer. *Gasmet Technologies*. http://www.gasmet.com/products/portable-gas-analyzers/dx4040 (accessed April 2018).

(14) TOCAM and Frog 5000 Portable GCs. *Defiant Technologies*. http://www.defiant-tech.com (accessed Nov 2018).

(15) Dräger X-pid Series. *Bentekk*. https://www.bentekk.com/en/x-pid/ (accessed Aug 2018).

(16) Lu, C. J.; Steinecker, W. H.; Tian, W. C.; Oborny, M. C.; Nichols, J. M.; Agah, M.; Potkay, J. A.; Chan, H. K.; Driscoll, J.; Sacks, R. D.; Wise, K. D.; Pang, S. W.; Zellers, E. T. *Lab Chip* **2005**, *5*, 1123−1131.

(17) Qin, Y.; Gianchandani, Y. B. *Microsyst. Nanoeng.* **2016**, *2*, 15049.

(18) Garg, A.; Akbar, M.; Vejerano, E.; Narayanan, S.; Nazhandali, L.; Marr, L. C.; Agah, M. *Sens. Actuators, B* **2015**, *212*, 145−154.

(19) Collin, W. R.; Bondy, A.; Paul, D.; Kurabayashi, K.; Zellers, E. T. *Anal. Chem.* **2015**, *87*, 1630−1637.

(20) Manginell, R. P.; Bauer, J. M.; Moorman, M. W.; Sanchez, L. J.; Anderson, J. M.; Whiting, J. J.; Porter, D. A.; Copic, D.; Achyuthan, K. E. *Sensors* **2011**, *11*, 6517−6532.

(21) Lewis, P. R.; Manginell, P.; Adkins, D. R.; Kottenstette, R.; Wheeler, D.; Sokolowski, S. S.; Trudell, D. E.; Byrnes, J. E.; Okandan, M.; Bauer, J. M.; Manley, R.; Frye-Mason, C. *IEEE Sens. J.* **2006**, *6*, 784−795.

(22) Zampolli, S.; Elmi, I.; Mancarella, F.; Betti, P.; Dalcanale, E.; Cardinali, G. C.; Severi, M. *Sens. Actuators, B* **2009**, *141*, 322−328.

(23) Kim, K. S.; Chang, H.; Zellers, E. T. *Anal. Chem.* **2011**, *83*, 7198−7206.

(24) Collin, W. R.; Serrano, G.; Wright, L. K.; Chang, H.; Nuñovero, N.; Zellers, E. T. *Anal. Chem.* **2014**, *86*, 655−663.

(25) Wang, J.; Bryant-Genevier, J.; Nunovero, N.; Zhang, C.; Kraay, B.; Zhan, C.; Scholten, K.; Nidetz, R.; Buggaveeti, S.; Zellers, E. T. *Microsyst. Nanoeng.* **2018**, *4*, 17101.

(26) Wright, L. K.; Zellers, E. T. *Analyst* **2013**, *138*, 6860−6868.

(27) Bryant-Genevier, J.; Zellers, E. T. *J. Chrom. A* **2015**, *1422*, 299−309.

(28) Lin, Z.; Nuñovero, N.; Wang, J.; Nidetz, R.; Buggaveeti, S.; Kurabayashi, K.; Zellers, E. T. *Sens. Actuators, B* **2018**, *254*, 561−572.

(29) Wang, J.; Nuñovero, N.; Lin, Z.; Nidetz, R.; Buggaveeti, S.; Zhan, C.; Kurabayashi, K.; Steinecker, W. H.; Zellers, E. T. *Procedia Eng.* **2016**, *168*, 1398−1401.

(30) Wang, J.; Nuñovero, N.; Zhan, C.; Nidetz, R.; Steinecker, W. H.; Peterson, S. J.; Brookover, B. H.; Zellers, E. T. *Proceedings* **2017**, *1*, 633.

(31) Rowe, M. P.; Plass, K. E.; Kim, K.; Kurdak, C.; Zellers, E. T.; Matzger, A. J. *Chem. Mater.* **2004**, *16*, 3513−3517.

(32) Jian, R. S.; Huang, R.; Lu, C. J. *Talanta* **2012**, *88*, 160−167.

(33) Reidy, S.; Lambertus, G.; Reece, J.; Sacks, R. *Anal. Chem.* **2006**, *78*, 2623−2630.

(34) Serrano, G.; Reidy, S.; Zellers, E. T. *Sens. Actuators, B* **2009**, *141*, 217−226.

(35) Brown, J.; Shirey, B. *A Tool for Selecting an Adsorbent for Thermal Desorption Applications*; T402025; Supelco: Bellefonte, PA, 2001.

(36) Jin, C.; Zellers, E. T. *Anal. Chem.* **2008**, *80*, 7283−7293.

DOI: 10.1021/acs.analchem.9b00263
Anal. Chem. 2019, 91, 4747−4754